Accurate modelling of orbital velocities near seabed using a nonlinear dispersive wave model

Baris BARLAS[1], Serdar BEJI[2] and Kazuo NADAOKA[3]
[1]Department of Naval Architecture and Ocean Engineering,
Istanbul Technical University, Maslak 80626, Istanbul, Turkey.
Fax: +(90) 212-285 6454
E-mail: barlas@itu.edu.tr
[2]Department of Naval Architecture and Ocean Engineering,
Istanbul Technical University, Maslak 80626, Istanbul, Turkey.
Fax: +(90) 212-285 6454
E-mail: sbeji@itu.edu.tr
[3]Graduate School of Information Science and Engineering,
Tokyo Institute of Technology, 2-12-1 O-okayama, Meguro-ku, Tokyo 152, Japan.
Fax: +(81) 3-3729-0728
E-mail: nadaoka@mei.titech.ac.jp

Abstract

The recently proposed nonlinear wave model of Nadaoka *et. al.* (1997) is re-expressed in boundary fitted non-orthogonal curvilinear co-ordinate system for simulating wave motions in domains with irregular boundaries. The co-ordinate transformation converts an irregular physical domain into a rectangular computational domain, which allows for accurate numerical computations using finite-differences approximations. Thus, the boundary conditions for irregular vertical enclosures surrounding a typical physical domain, such as a port or harbour, are satisfied accurately. This improved numerical treatment of the boundaries increase the accuracy of wave model predictions of the velocities inside the domain and on the vertical enclosures, which in turn results in better estimation of wave orbital velocities over the entire water depth. Comparisons of computational results with experimental measurements of horizontal and vertical orbital velocities of nonlinear unidirectional waves propagating over a submarine bar show good agreement and prove the superiority of the new wave model over an improved Boussinesq model. These comparisons are taken to be indicative of the same order of accuracy for orbital velocity predictions of directional wave motions, which are important for sediment transport predictions.

1.Wave Model

The wave model adopted in this work is the single-component form of the fully-dispersive weakly-nonlinear wave equations of Nadaoka *et. al.* (1997). The wave model is valid for arbitrary depths, ranging from infinitely deep to very shallow waters. Thus, the model is capable of simulating the second-order Stokes waves and cnoidal waves equally well. The corresponding single-component forms of the continuity and momentum equations of the wave model are

$$\frac{\partial \zeta}{\partial t} + \nabla \cdot \left[\left(\frac{C_p^2}{g} + \zeta \right) \vec{u} \right] = 0 \quad , (1)$$

$$C_p C_g \frac{\partial \vec{u}}{\partial t} + C_p^2 \nabla \left[g\zeta + \zeta \frac{\partial w}{\partial t} + \frac{1}{2} \left(\vec{u} \cdot \vec{u} + w^2 \right) \right] = \frac{\partial}{\partial t} \left[\frac{C_p \left(C_p - C_g \right)}{k^2} \nabla \left(\nabla \cdot \vec{u} \right) + \nabla \left(\frac{C_p \left(C_p - C_g \right)}{k^2} \right) \left(\nabla \cdot \vec{u} \right) \right] \quad (2)$$

where $\vec{u}$ is the horizontal velocity vector and w the vertical component of velocity both at z=0. ζ is the free surface elevation, h the local water depth as measured from the still water level, and ∇ the horizontal gradient operator with (∂/∂ x,∂/∂ y) components. C_P, C_g, and k denote respectively the phase and group velocities and wave number, computed according to the linear theory for a prescribed dominant frequency ω and a given local depth h.

2. Transformed Wave Equations

The boundary fitted curvilinear co-ordinate system (ξ ,η), as seen in Figure 1, is now introduced. Here, ξ is taken usually (not necessarily) in the direction of wave propagation while η is taken perpendicular to the ξ lines.

Figure 1: A typical example for co-ordinate transformation from the physical domain to the computational domain.

The wave equations are transformed from the physical space (x, y) to the computational space (ξ ,η) by the following co-ordinate transformation relations Hoffman and Chiang (1995):

$$\tau = t, \qquad \xi = \xi(t,x,y), \qquad \eta = \eta(t,x,y)$$

$$\frac{\partial}{\partial t} = \frac{\partial}{\partial \tau}, \qquad \frac{\partial}{\partial x} = \xi_x \frac{\partial}{\partial \xi} + \eta_x \frac{\partial}{\partial \eta}, \qquad \frac{\partial}{\partial y} = \xi_y \frac{\partial}{\partial \xi} + \eta_y \frac{\partial}{\partial \eta} \quad (3)$$

The continuity (1) and momentum equations (2) are re-expressed in a general, curvilinear non-orthogonal co-ordinates through above transformations; however, the Cartesian velocity components are not transformed therefore the components of the momentum equation is still in Cartesian directions. This gives strong conservative formulation with less metric coefficients in the transformed equations, which read

$$\frac{\partial \zeta}{\partial \tau} + \xi_x \frac{\partial P}{\partial \xi} + \eta_x \frac{\partial P}{\partial \eta} + \xi_y \frac{\partial Q}{\partial \xi} + \eta_y \frac{\partial Q}{\partial \eta} = 0 \quad , (4)$$

for continuity, and

$$C \cdot \xi_x^2 \frac{\partial^3 u}{\partial \xi^2 \partial \tau} + CX \cdot \xi_x \frac{\partial^2 u}{\partial \xi \partial \tau} - R \cdot \frac{\partial u}{\partial \tau} = RHSX \quad (5)$$

$$C \cdot \eta_y^2 \frac{\partial^3 v}{\partial \eta^2 \partial \tau} + CY \cdot \eta_y \frac{\partial^2 v}{\partial \eta \partial \tau} - R \cdot \frac{\partial v}{\partial \tau} = RHSY \quad (6)$$

for x- and y- momentum equations, respectively. Here, u, v are the velocity components at the still water level in the Cartesian coordinates. P, Q, R, C, CX, CY, RHSX, and RHSY are defined as

$$C = \frac{C_p^2 (1 - R)}{\omega^2} \quad (7a)$$

$$CX = \frac{1}{\omega^2}\left(\xi_x \frac{\partial}{\partial \xi}\left(C_p^2(1-R)\right) + \eta_x \frac{\partial}{\partial \eta}\left(C_p^2(1-R)\right)\right) \quad (7b)$$

$$CY = \frac{1}{\omega^2}\left(\xi_y \frac{\partial}{\partial \xi}\left(C_p^2(1-R)\right) + \eta_y \frac{\partial}{\partial \eta}\left(C_p^2(1-R)\right)\right) \quad (7c)$$

$$P = \left(\frac{C_p^2}{g} + \zeta\right)\cdot u \quad Q = \left(\frac{C_p^2}{g} + \zeta\right)\cdot v \quad R = \frac{C_g}{C_p} \quad (7d)$$

$$\begin{aligned} RHSX = {} & \xi_x \frac{\partial S}{\partial \xi} + \eta_x \frac{\partial S}{\partial \eta} \\ & - C\cdot\left(\xi_{xy}\frac{\partial^2 v}{\partial \tau \partial \xi} + \eta_{xy}\frac{\partial^2 v}{\partial \tau \partial \eta} + \xi_x\xi_y\frac{\partial^3 v}{\partial \tau \partial \xi^2} + \eta_x\eta_y\frac{\partial^3 v}{\partial \tau \partial \eta^2} + \xi_x\eta_y\frac{\partial^3 v}{\partial \tau \partial \xi \partial \eta} + \eta_x\xi_y\frac{\partial^3 v}{\partial \tau \partial \xi \partial \eta}\right) \\ & - C\cdot\left(\eta_x^2\frac{\partial^3 u}{\partial \tau \partial \eta^2} + 2\xi_x\eta_x\frac{\partial^3 u}{\partial \tau \partial \xi \partial \eta} + \xi_{xx}\frac{\partial^2 u}{\partial \tau \partial \xi} + \eta_{xx}\frac{\partial^2 u}{\partial \tau \partial \eta}\right) \\ & - CX\cdot\left(\xi_y\frac{\partial^2 v}{\partial \tau \partial \xi} + \eta_y\frac{\partial^2 v}{\partial \tau \partial \eta} + \eta_x\frac{\partial^2 u}{\partial \tau \partial \eta}\right) \end{aligned} \quad (8a)$$

$$\begin{aligned} RHSY = {} & \xi_y \frac{\partial S}{\partial \xi} + \eta_y \frac{\partial S}{\partial \eta} \\ & - C\cdot\left(\xi_{xy}\frac{\partial^2 u}{\partial \tau \partial \xi} + \eta_{xy}\frac{\partial^2 u}{\partial \tau \partial \eta} + \xi_x\xi_y\frac{\partial^3 u}{\partial \tau \partial \xi^2} + \eta_x\eta_y\frac{\partial^3 u}{\partial \tau \partial \eta^2} + \xi_x\eta_y\frac{\partial^3 u}{\partial \tau \partial \xi \partial \eta} + \eta_x\xi_y\frac{\partial^3 u}{\partial \tau \partial \xi \partial \eta}\right) \\ & - C\cdot\left(\eta_x^2\frac{\partial^3 v}{\partial \tau \partial \eta^2} + 2\xi_x\eta_x\frac{\partial^3 v}{\partial \tau \partial \xi \partial \eta} + \xi_{xx}\frac{\partial^2 v}{\partial \tau \partial \xi} + \eta_{xx}\frac{\partial^2 v}{\partial \tau \partial \eta}\right) \\ & - CY\cdot\left(\xi_y\frac{\partial^2 u}{\partial \tau \partial \xi} + \eta_y\frac{\partial^2 u}{\partial \tau \partial \eta} + \eta_x\frac{\partial^2 v}{\partial \tau \partial \eta}\right) \end{aligned} \quad (8b)$$

ξ_x, ξ_y, ... appearing in equations (3)-(7) are the grid metrics, and S is given by

$$S = g\cdot\zeta + \zeta\frac{\partial w}{\partial \tau} + \frac{1}{2}\left(u^2 + v^2 + w^2\right) \quad (9)$$

3. Numerical Approach

The transformed continuity and momentum equations (4-5-6) are discretized by finite difference approximations using non-staggered grids, where the free surface displacement, the velocity components, and the grid metrics are defined at the grid intersections. The second-order central-difference formulae are used for approximating all the partial derivatives both in time and space. The basic algorithm is divided into two stages: In the first stage, the velocity components are computed by solving the momentum equations (5-6) until a specific convergence criterion

is met. The solution of the velocity components requires the use of Thomas algorithm, which is quite efficient in the solution of tridiagonal matrix systems. Then, using the final velocity components, the free surface elevation is obtained from the continuity equation (4) at each time step. See Beji and Nadaoka (1995) for a similar approach.

The boundary conditions on the free surface and on the bottom are automatically satisfied by the wave equations. It then remains to specify the conditions on the incident and outgoing boundary and on the vertical enclosures surrounding the domain. The conditions at the incoming boundary are easily specified by introducing an incident wave field; likewise, the wall condition, which states that the velocity normal to the wall surface must vanish, is satisfied easily in the transformed rectangular computational domain. The radiation condition usually presents difficulties since there is no perfect radiation condition for nonlinear directional waves leaving the domain. Here, the second-order radiation condition of Engquist and Majda (1977) is used to minimise the artificially reflected waves from the outgoing boundary.

A sample computation using the above scheme for the case of wave propagation over a topographical lens (Whalin, 1972) is performed. The bathymetry is given as

$$h(x,y) = \begin{cases} 0.4572 & \text{for} \quad 0 \le x < 10.67 - G \\ 0.4572 + (10.67 - G - x)/25 & \text{for} \quad 10.67 - G \le x < 18.29 - G \\ 0.1524 & \text{for} \quad 18.29 - G \le x \le 21.34 \end{cases} \tag{10}$$

where $G(y) = [y(6.096 - y)]^{n_1}$ for $0 \le y \le 6.096$. Figure 2 shows the bathymetry according to these definitions.

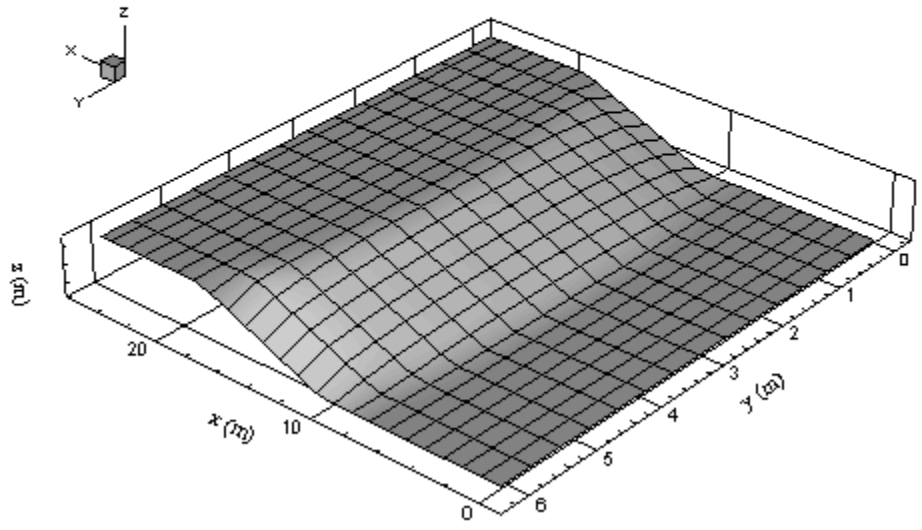

Figure 2: A perspective view of the bathymetry for Whalin's experiments.

Since the physical domain itself in this case is rectangular, this simulation should be regarded as a simple testing of the general numerical scheme for the special case of a rectangular domain. Among the various measurements we have chosen the case for incident waves of T=2 seconds period and a=0.75 cm amplitude. Figure 3 shows the fully-developed wave field over this bathymetry and Figure 4 shows the comparisons with Whalin's measurements for harmonic amplitudes along the centerline of the wave basin. As it can be seen from Figure 4, the wave model predictions agree considerably well with the measurements hence show that the general model developed here works correctly for the special case of a rectangular domain.

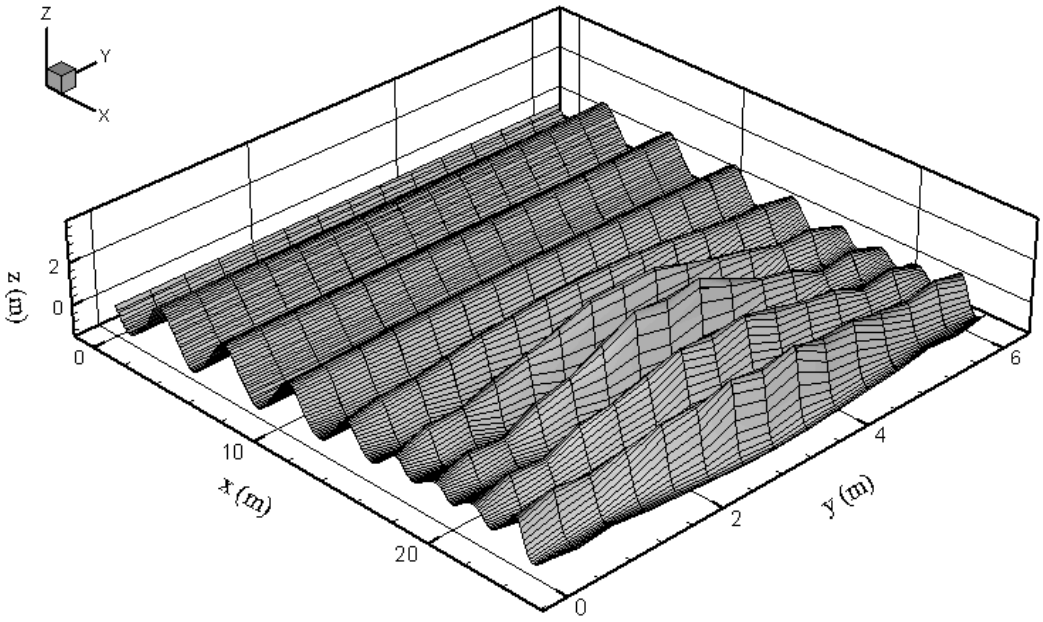

Figure 3: A perspective view of the fully-developed wave field for incident waves of T=2 seconds period and a=0.75 cm amplitude.

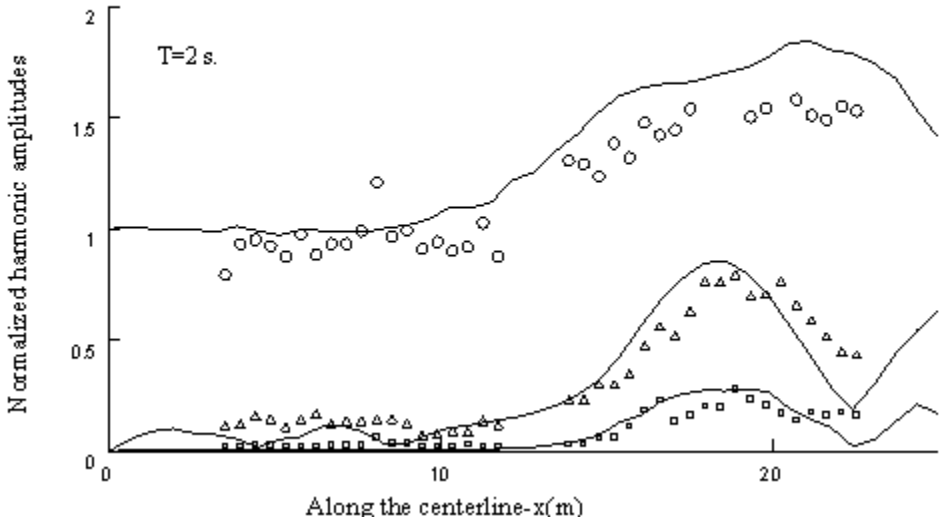

Figure 4: Comparisons of the computed harmonic amplitudes with Whalin's measurements for incident waves of T=2 seconds period and a=0.75 cm amplitude. Solid line: computation, scatter: measurement (circle: first harmonic, triangle: second harmonic, and square: third harmonic).

4. Comparisons with Experimental Measurements of Orbital Velocities

In order to test the reliability of the wave model adopted in this work, a series of measurements of horizontal and vertical orbital velocities for nonlinear waves propagating over a submarine bar (Nadaoka *et. al.*, 1994) is now compared with the computations using the 1-D forms of the wave equations. Also, comparisons are made with the predictions of an improved Boussinesq model (Madsen and Sørensen, 1992; Beji and Nadaoka, 1996). The results clearly show the superiority of the present wave model over the improved Boussinesq model, which usually is regarded as one of the most reliable models for simulating wave motions in the near shore zone.

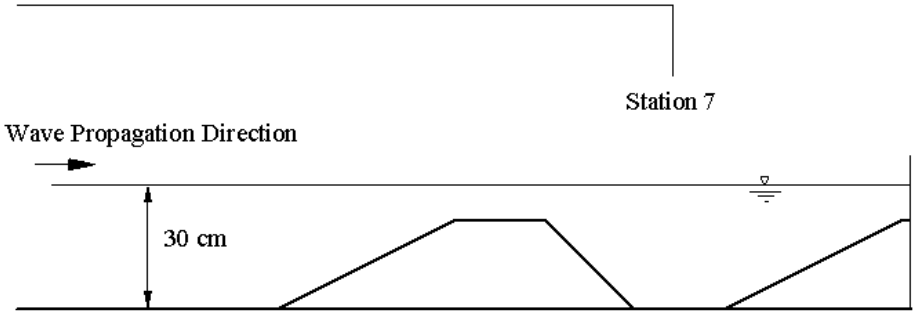

Figure 5: Definition sketch of the wave flume for nonlinear wave propagation over a submarine bar. Incident wave height is 2cm and wave period is 1.5 s.

The experimental setup consists of a submerged bar with an upslope of 1:20, followed by a horizontal crest of 2m long and a downslope of 1:10. The water depth in the deepest section is 0.3m, which reduces to 0.1m over the horizontal crest and again increases to 0.3 m behind the bar, as seen in Figure 5.

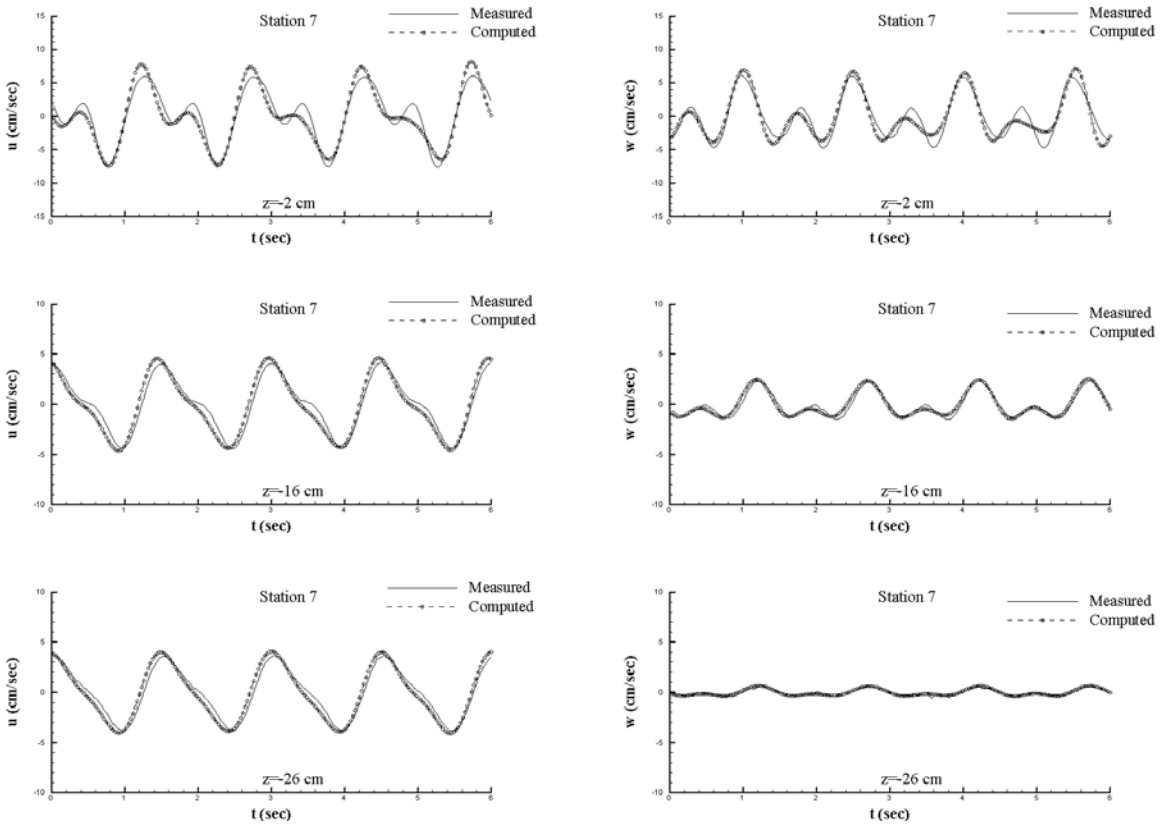

Figure 6: Comparisons of the computational results using the wave model adopted in this work with the experimental measurements of horizontal and vertical velocity components at station 7 behind the submerged bar. Left column horizontal velocities and right column vertical velocities at z=2cm, z=16cm and z=26cm below the still water level.

The experimental data compared here is for waves with incident wave height H=2cm and period T=1.5s. Since the waves steepening in the shallowest section are decomposed into their harmonics behind the bar, the waves observed at station 7 include shorter free waves, which may be classified as deep water waves. This important aspect requires a wave model with good dispersion characteristics in order to predict velocities accurately. Here, we compare the computations results of our wave model and those of the improved Boussinesq model with the experimental measurements of orbital velocities at station 7 only since this particular station represents the most challenging case

among all others due to the reasons indicated above. The comparisons are given for three different water depths; that is, 2cm, 16cm, and 26cm below the still water level.

As seen above in Figure 6, the predictions of the model simulations agree well with the experimental measurements both for horizontal and vertical velocity components at all the water levels. The same comparisons, performed using the improved Boussinesq model, are given below in Figure 7. However, the results do not agree with the measurements as well as the previous computations do. Thus, these comparisons clearly show the superiority of the present model over the improved Boussinesq model in predicting the orbital velocities for complicated wave transformations. This point is essential in making accurate computations of sediment transport rate due to waves.

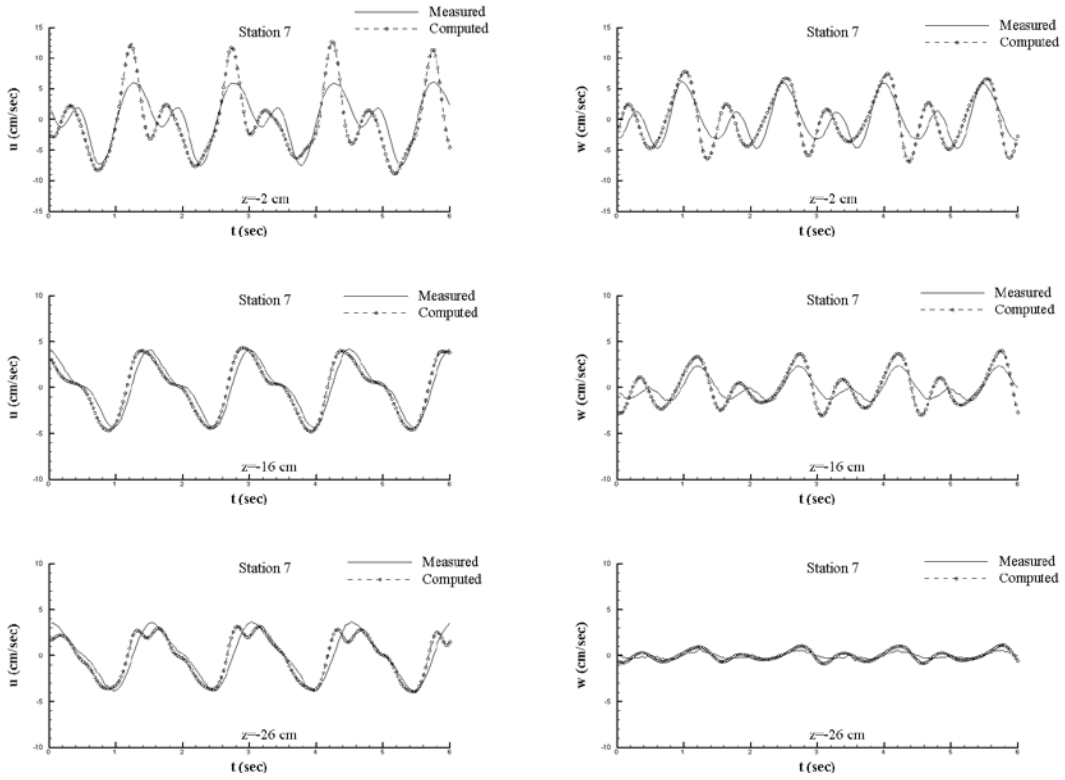

Figure 7: Comparisons of the computational results using the improved Boussinesq model with the experimental measurements of horizontal and vertical velocity components at station 7 behind the submerged bar. Left column horizontal velocities; right column vertical velocities at z=2cm, z=16cm and z=26cm below the still water level.

Conclusion

The recently developed nonlinear wave model of Nadaoka *et.al.* (1997) has been re-expressed in the boundary fitted curvilinear co-ordinate system to achieve accurate treatment of the boundary conditions for irregular physical domains. The numerical scheme based on the transformed wave equations is used for a sample simulation of nonlinear wave propagation over a topographical lens and the results are found to be quite acceptable. Furthermore, for the special case of 1-D motion, the numerical simulations of orbital velocities behind a submerged bar are compared with the measurements of Nadaoka *et. al.* (1994). The results are very satisfactory and clearly better than the simulations performed with a Boussinesq model. Thus, it may be concluded that the model adopted here shows

promising aspects for using it in future practical application, especially in the estimation of sediment transport rates via orbital velocities.

References:

- Beji, S. and Nadaoka, K., 1995. Directional wave simulations by a new time-dependent nonlinear mild-slope equation. *Proc. 2nd Int. Conf. MEDCOAST'95*, Tarragona, Spain, **3**, 1929-1943.
- Beji, S. and Nadaoka, K., 1996. A formal derivation and numerical modelling of the improved Boussinesq equations for varying depth. *Ocean Engineering*, **23-8**, 691-704.
- Engquist, B. and Majda, A., 1977. Absorbing boundary conditions for the numerical simulation of waves. *Math. Comp*. **31**, 629-651.
- Hoffmann, K.A. and Chiang, S.T., 1995. *Computational Fluid Dynamics for Engineers* – Volume: **1**, **2**, Engineering Education System Publication, Wichita.
- Madsen, P.A. and Sørensen, O.R., 1992. A new form of the Boussinesq equations with improved linear dispersion characteristics. Part 2: A slowly-varying bathymetry. *Coastal Engineering*, **18**, 183-204.
- Nadaoka, K., Beji, S. and Nakagawa, Y., 1994. A fully-dispersive nonlinear wave model and its numerical solutions. *Proc. 24th Int. Conf. Coastal Eng.*, **1**, 427-441.
- Nadaoka, K., Beji, S. and Nakagawa, Y., 1997. A fully dispersive weakly nonlinear model for water waves, *Proc. Royal Soc.*, London, Ser A, **453**, 303-308.
- Whalin, R.W., 1971. The Limit of Applicability of Linear Refraction Theory in a Convergence Zone. *Res. Rep. H-71-3*, U.S. Army Corps of Engrs., Waterways Expt. Station, Vicksburg, M.S.

Sommaire: